Peer-reviewed version available at *Materials* **2020**, *13*, 2527; doi:10.3390/ma13112527

The meshless analysis of scale dependent problems for coupled fields

Jan Sladek[1], Vladimir Sladek[1] and Pihua H. Wen[2]

[1] Institute of Construction and Architecture, Slovak Academy of Sciences, 84503 Bratislava, Slovakia
[2] School of Engineering and Materials Sciences, Queen Mary University of London, Mile End, London E14NS, U.K.

Abstract. The meshless Petrov-Galerkin (MLPG) method is developed to analyse 2-D problems for flexoelectricity and thermoelectricity. Both problems are multiphysical and scale dependent. The size-effect is considered by the strain- and electric field-gradients in the flexoelecricity and higher-grade heat flux in the thermoelectricity. The variational principle is applied to derive the governing equations considered constitutive equations. The order of derivatives in governing equations is higher than in equations obtained from classical theory. The coupled governing partial differential equations (PDE) are satisfied in a local weak-form on small fictitious subdomains with a simple test function. Physical fields are approximated by the moving least-squares (MLS) scheme. Applying the spatial approximations in local integral equations a system of algebraic is obtained for the nodal unknowns.

Keywords: MLS approximation, Gradients of strains, Gradients of electric intensity vector, Higher-grade heat flux

1. Introduction

In nanocomposites the nano-sized particles are incorporated into a matrix. In these materials the ratio of surface to volume is significantly larger than in their bulk-sized equivalent. Then, their properties can be many times improved with respect to those known for the component parts. The mechanical strength, toughness and electrical or thermal conductivity can be drastically improved in nanocomposites. Therefore, they are starting to be intensively utilized in many engineering fields. However, in nano-sized structures it is observed the size-effect phenomena if the characteristic length of material structure is compared with the size of the analyzed body [1-5]. Even some new phenomena are observed in nano-sized structures, like electric polarization in centro-symmetric crystals. It is explained by the direct flexoelectricity effect [6-8]. With respect to piezoelectricity, it can be viewed as a higher order effect [9]. If stresses are proportional

Peer-reviewed version available at *Materials* **2020**, *13*, 2527; doi:10.3390/ma13112527

to the gradients of electric intensity vector, we are talking about the converse flexoelectricity [10-12]. The strain- and electric intensity vector- gradients are very large in nano-sized dielectrics and they should be considered in constitutive equations.

Nanotechnology is also successfully utilized in improving of thermoelectric properties [13]. Thermoelectric materials have a potential to convert waste heat directly into electricity if the thermal conductivity is reduced without affecting the high electrical conductivity [14]. The thermal conductivity is reduced significantly in nanostructures only. Scattering of phonons is observed only on interfaces of nanostructures. Due to scattering of phonons the thermal conductivity is reduced. Since the electrons are smaller, they are not scattered and the electric conductivity is not reduced. It requires to develop a theory for heat conduction, where size effect is considered. The microstructural material characteristics are not considered in the classical continuum mechanics and results are size-independent. Atomistic models are able to consider the size-effect in structural elements. However, extremely high requirements are put on computer memory in this approach. It is more convenient to develop advanced continuum models, where the intrinsic length parameter (characteristic of material microstructure) is considered [15-17]. Former gradient theory is very complicated due to many length scales as material parameters, which are not available. Therefore, Aifantis [18] simplified former theory by introducing only one length parameter. The nonlocality should be considered in the heat conduction problems if the temperature gradients are large [19]. For a special weight function in nonlocal integral expression of the heat flux vector it is possible to transform the integral form into a differential equation with a characteristic length parameter representing the nonlocality. In both flexoelectric and thermoelectric problems, we have constitutive equations with the intrinsic material parameter representing microstructure and higher derivatives of physical fields than in corresponding problems described by classical theory. In both problems there are interactions of several physical fields.

It is needed to have a reliable and accurate computational tool to solve these multiphysical problems described by gradient theories with intrinsic material parameters. Higher order derivatives in governing equations require the C^1-continuous elements in numerical domain discretization methods to guarantee the continuity of variables and their derivatives on interfaces of elements. It is a difficult task to obey such a requirement. It is more convenient to develop the mixed formulation in the finite element method (FEM) [20, 21]. The order of continuity of the Moving Least-square (MLS) approximation in the Meshless Local Petrov-Galerkin method (MLPG) can be tuned to a desired value very easily [22-24].

In the present paper, the authors have developed a meshless method based on the MLPG weak-form to solve multiphysical problems in dielectric and thermoelectric solids. Both the direct and converse flexoelectricity is considered in dielectric solids. Nodal points are spread on the analyzed domain and each node is surrounded by a small circle for simplicity, but without loss of generality. The spatial variations of primary physical fields are approximated by the moving least-squares (MLS) scheme. After performing the spatial integrations, a system of algebraic or ordinary differential equations for unknown nodal values is obtained. The essential boundary conditions on the global boundary are satisfied by the collocation. Numerical examples are presented and discussed to compare the results obtained by the gradient theory with those obtained by classical theory.

2. The MLPG for flexoelectricity

2.1 The direct and converse flexoelectricity

The electric enthalpy density for piezoelectric solids with strain and electric intensity vector gradients and can be written as [25, 26]

$$H = \frac{1}{2}c_{ijkl}\varepsilon_{ij}\varepsilon_{kl} - \frac{1}{2}a_{ij}E_iE_j - e_{kji}\varepsilon_{ij}E_k + \frac{1}{2}g_{jklmni}\eta_{jkl}\eta_{mni} - f_{ijkl}E_i\eta_{jkl} + \\ + b_{klij}\varepsilon_{ij}E_{k,l} - \frac{1}{2}h_{ijkl}E_{i,j}E_{k,l}\,, \tag{1}$$

where **a** and **c** denote the second-order permittivity and the fourth-order elastic constant tensors, respectively. Symbols **e** and **f** are used for the piezoelectric and flexoelectric coefficients, respectively. Symbol **g** denotes the higher order elastic coefficients. Finally, the symbols **b** and **h** are used for the converse flexoelectric coefficients and higher-order electric parameters, respectively.

The strain tensor ε_{ij} and the electric field vector E_j are related to the displacements u_i and the electric potential ϕ by

$$\varepsilon_{ij} = \frac{1}{2}\left(u_{i,j} + u_{j,i}\right), \quad E_j = -\phi_{,j}\ . \tag{2}$$

The strain-gradients are denoted by symbol $\boldsymbol{\eta}$

$$\eta_{ijk} = \varepsilon_{ij,k} = \frac{1}{2}\left(u_{i,jk} + u_{j,ik}\right)\ . \tag{3}$$

The constitutive equations are obtained from the electric enthalpy density expression (1) as

Preprints (www.preprints.org) | NOT PEER-REVIEWED | Posted: 6 May 2020 doi:10.20944/preprints202005.0095.v1

Peer-reviewed version available at Materials 2020, 13, 2527; doi:10.3390/ma13112527

$$\sigma_{ij} = \frac{\partial H}{\partial \varepsilon_{ij}} = c_{ijkl}\varepsilon_{kl} - e_{kij}E_k - b_{klij}E_{k,l},$$

$$\tau_{jkl} = \frac{\partial H}{\partial \eta_{jkl}} = -f_{ijkl}E_i + g_{jklmni}\eta_{nmi},$$

$$D_i = -\frac{\partial H}{\partial E_i} = a_{ij}E_j + e_{ijk}\varepsilon_{jk} + f_{ijkl}\eta_{jkl},$$

$$Q_{ij} = -\frac{\partial H}{\partial E_{i,j}} = b_{ijkl}\varepsilon_{kl} + h_{ijkl}E_{k,l}, \quad (4)$$

where σ_{ij}, D_k, τ_{jkl} and Q_{ij} are the stress tensor, electric displacements, higher order stress and electric quadrupole, respectively.

In the simplified gradient theory [18, 27, 28] only one internal length-scale parameter l is present. Then, the higher-order elastic parameters g_{jklmni} are proportional to the conventional elastic stiffness coefficients c_{klmn} and the length material parameter l [29,30] as

$$g_{jklmni} = l^2 c_{jkmn}\delta_{li}, \quad (5)$$

with δ_{li} being the Kronecker delta.

A similar idea of simplification has been applied to the higher-order electric parameters

$$h_{ijkl} = q^2 a_{ik}\delta_{jl}, \quad (6)$$

where q is another length-scale parameter.

In the simplified direct flexoelectricity there are considered two independent parameters f_1 and f_2 for the direct flexoelectric coefficient f_{ijkl}, $f_{ijkl} = f_1\delta_{jk}\delta_{il} + f_2\left(\delta_{ij}\delta_{kl} + \delta_{ik}\delta_{jl}\right)$ [20]. Taking into account the above simplifications, the electric enthalpy density can be written as

$$H = \frac{1}{2}c_{ijkl}\varepsilon_{ij}\varepsilon_{kl} - \frac{1}{2}a_{ij}E_iE_j - e_{kji}\varepsilon_{ij}E_k + \frac{l^2}{2}c_{jkmn}\eta_{jkl}\eta_{mnl} - f_1E_i\eta_{kki} - f_2E_i\left(\eta_{ikk} + \eta_{jij}\right) +$$

$$+ b_{klij}\varepsilon_{ij}E_{k,l} - \frac{q^2}{2}a_{ik}E_{i,j}E_{k,j}. \quad (7)$$

Finally, we reduce the number of independent converse flexoelectric coefficients b_{ijkl}. The stresses induced by electric intensity vector in the orthotropic piezoelectric material with poling direction along the transversal isotropy x_3-axis can be written as

$$\sigma_{11} = e_{31}E_3, \quad \sigma_{33} = e_{33}E_3, \quad \sigma_{13} = e_{15}E_1,$$

Preprints (www.preprints.org) | NOT PEER-REVIEWED | Posted: 6 May 2020 doi:10.20944/preprints202005.0095.v1

Peer-reviewed version available at Materials 2020, 13, 2527; doi:10.3390/ma13112527

with $e_{kij} = \left(e_{31}\delta_{i1}\delta_{j1} + e_{33}\delta_{i3}\delta_{j3}\right)\delta_{k3} + e_{15}\left(\delta_{i1}\delta_{j3} + \delta_{i3}\delta_{j1}\right)\delta_{k1}$ (8)

where standard Voight notation is applied (Sladek et al. 2018).

A similar form is considered for induced stresses induced by the converse flexoelectricity

$$\sigma_{ij} = \delta_{ij} b_1 \left(E_{1,1} + E_{3,3}\right), \quad \sigma_{13} = \sigma_{31} = b_2 E_{1,3} + b_3 E_{3,1} \tag{9}$$

with three independent converse flexoelectric coefficients b_1, b_2 and b_3 by $b_{klij} = b_1\delta_{ij}\delta_{kl} + \left(\delta_{i1}\delta_{j3} + \delta_{i3}\delta_{j1}\right)\left(b_2\delta_{k1}\delta_{l3} + b_3\delta_{k3}\delta_{l1}\right)$.

Then, the final form of the electric enthalpy is given by

$$\begin{aligned} H = {} & \frac{1}{2}c_{ijkl}\varepsilon_{ij}\varepsilon_{kl} - \frac{1}{2}a_{ij}E_iE_j - e_{31}\varepsilon_{11}E_3 - e_{33}\varepsilon_{33}E_3 - e_{15}\left(\varepsilon_{13} + \varepsilon_{31}\right)E_1 + \frac{l^2}{2}c_{jkmn}\eta_{jkl}\eta_{mnl} - \\ & - f_1E_i\eta_{kki} - f_2E_i\left(\eta_{ikk} + \eta_{jij}\right) + b_1\varepsilon_{kk}E_{i,i} + \left(b_2E_{1,3} + b_3E_{3,1}\right)\left(\varepsilon_{13} + \varepsilon_{31}\right) - \frac{q^2}{2}a_{ik}E_{i,j}E_{k,j} \end{aligned} . \tag{10}$$

The constitutive equations (4) for orthotropic materials can be rewritten into a matrix form as

$$\begin{bmatrix}\sigma_{11}\\ \sigma_{33}\\ \sigma_{13}\end{bmatrix} = \begin{bmatrix}c_{11} & c_{13} & 0\\ c_{13} & c_{33} & 0\\ 0 & 0 & c_{44}\end{bmatrix}\begin{bmatrix}\varepsilon_{11}\\ \varepsilon_{33}\\ 2\varepsilon_{13}\end{bmatrix} - \begin{bmatrix}0 & e_{31}\\ 0 & e_{33}\\ e_{15} & 0\end{bmatrix}\begin{bmatrix}E_1\\ E_3\end{bmatrix} - \begin{bmatrix}b_1 & 0\\ b_1 & 0\\ 0 & b_3\end{bmatrix}\begin{bmatrix}E_{1,1}\\ E_{3,1}\end{bmatrix} - \begin{bmatrix}0 & b_1\\ 0 & b_1\\ b_2 & 0\end{bmatrix}\begin{bmatrix}E_{1,3}\\ E_{3,3}\end{bmatrix} =$$

$$= \mathbf{C}\begin{bmatrix}\varepsilon_{11}\\ \varepsilon_{33}\\ 2\varepsilon_{13}\end{bmatrix} - \mathbf{\Lambda}\begin{bmatrix}E_1\\ E_3\end{bmatrix} - \mathbf{\Phi}_1\begin{bmatrix}E_{1,1}\\ E_{3,1}\end{bmatrix} - \mathbf{\Phi}_3\begin{bmatrix}E_{1,3}\\ E_{3,3}\end{bmatrix}, \tag{11}$$

$$\begin{bmatrix}D_1\\ D_3\end{bmatrix} = \begin{bmatrix}0 & 0 & e_{15}\\ e_{31} & e_{33} & 0\end{bmatrix}\begin{bmatrix}\varepsilon_{11}\\ \varepsilon_{33}\\ 2\varepsilon_{13}\end{bmatrix} + \begin{bmatrix}a_1 & 0\\ 0 & a_2\end{bmatrix}\begin{bmatrix}E_1\\ E_3\end{bmatrix} +$$

$$+ \begin{bmatrix}f_1 + 2f_2 & f_1 & 0\\ 0 & 0 & f_2\end{bmatrix}\begin{bmatrix}\varepsilon_{11,1}\\ \varepsilon_{33,1}\\ 2\varepsilon_{13,1}\end{bmatrix} + \begin{bmatrix}0 & 0 & f_2\\ f_1 & f_1 + 2f_2 & 0\end{bmatrix}\begin{bmatrix}\varepsilon_{11,3}\\ \varepsilon_{33,3}\\ 2\varepsilon_{13,3}\end{bmatrix} =$$

$$= \mathbf{\Lambda}^T\begin{bmatrix}\varepsilon_{11}\\ \varepsilon_{33}\\ 2\varepsilon_{13}\end{bmatrix} + \mathbf{A}\begin{bmatrix}E_1\\ E_3\end{bmatrix} + \mathbf{F}_1\begin{bmatrix}\varepsilon_{11,1}\\ \varepsilon_{33,1}\\ 2\varepsilon_{13,1}\end{bmatrix} + \mathbf{F}_3\begin{bmatrix}\varepsilon_{11,3}\\ \varepsilon_{33,3}\\ 2\varepsilon_{13,3}\end{bmatrix}, \tag{12}$$

$$\begin{bmatrix}\tau_{11k}\\ \tau_{33k}\\ \tau_{13k}\end{bmatrix} = -\mathbf{F}_k^T\begin{bmatrix}E_1\\ E_3\end{bmatrix} + l^2\mathbf{C}\begin{bmatrix}\varepsilon_{11,k}\\ \varepsilon_{33,k}\\ 2\varepsilon_{13,k}\end{bmatrix}, \tag{13}$$

$$\begin{bmatrix} Q_{1k} \\ Q_{3k} \end{bmatrix} = \mathbf{\Phi}_k^T \begin{bmatrix} \varepsilon_{11} \\ \varepsilon_{33} \\ 2\varepsilon_{13} \end{bmatrix} + q^2 \mathbf{A} \begin{bmatrix} E_{1,k} \\ E_{3,k} \end{bmatrix}. \tag{14}$$

Using the variational principle of least action, it is possible to derive the governing equations for the considered constitutive equations [31]

$$\sigma_{ij,j}(\mathbf{x}) - \tau_{ijk,jk}(\mathbf{x}) = 0,$$

$$D_{i,i}(\mathbf{x}) - Q_{ij,ji}(\mathbf{x}) = 0. \tag{15}$$

Essential and natural boundary conditions (b.c.) follow from the variational formulation of boundary value problems:

1.) Essential b.c.: $u_i(\mathbf{x}) = \bar{u}_i(\mathbf{x})$ on Γ_u , $\Gamma_u \subset \Gamma$

$$s_i(\mathbf{x}) = \bar{s}_i \text{ on } \Gamma_s \text{ , } \Gamma_s \subset \Gamma \tag{16}$$

$$\phi(\mathbf{x}) = \bar{\phi}(\mathbf{x}) \text{ on } \Gamma_\phi \text{ , } \Gamma_\phi \subset \Gamma$$

$$p(\mathbf{x}) = \frac{\partial \phi}{\partial n} = \bar{p}(\mathbf{x}) \text{ on } \Gamma_p \text{ , } \Gamma_p \subset \Gamma$$

2.) Natural b.c.: $t_i(\mathbf{x}) = \bar{t}_i(\mathbf{x})$ on Γ_t , $\Gamma_t \cup \Gamma_u = \Gamma$, $\Gamma_t \cap \Gamma_u = \varnothing$

$$R_i(\mathbf{x}) = \bar{R}_i(\mathbf{x}) \text{ on } \Gamma_R \text{ , } \Gamma_R \cup \Gamma_s = \Gamma \text{ , } \Gamma_R \cap \Gamma_s = \varnothing \tag{17}$$

$$S(\mathbf{x}) = \bar{S}(\mathbf{x}) \text{ on } \Gamma_S \text{ , } \Gamma_S \cup \Gamma_\phi = \Gamma \text{ , } \Gamma_S \cap \Gamma_\phi = \varnothing$$

$$Z(\mathbf{x}) = \bar{Z}(\mathbf{x}) \text{ on } \Gamma_Z \text{ , } \Gamma_Z \cup \Gamma_p = \Gamma \text{ , } \Gamma_Z \cap \Gamma_p = \varnothing,$$

where $s_i := \frac{\partial u_i}{\partial \mathbf{n}}$, $p := \frac{\partial \phi}{\partial \mathbf{n}}$, $R_i := n_k n_j \tau_{ijk}$, $Z := n_i n_j Q_{ij}$, (18)

and the traction vector, and the electric charge are defined as

$$t_i := n_j \left(\sigma_{ij} - \tau_{ijk,k} \right) - \frac{\partial \rho_i}{\partial \boldsymbol{\pi}} + \sum_c \left\| \rho_i(\mathbf{x}^c) \right\| \delta(\mathbf{x} - \mathbf{x}^c), \tag{19}$$

$$S := n_k \left(D_k - Q_{kj,j} \right) - \frac{\partial \alpha}{\partial \boldsymbol{\pi}} + \sum_c \left\| \alpha(\mathbf{x}^c) \right\| \delta(\mathbf{x} - \mathbf{x}^c), \tag{20}$$

with $\rho_i := n_k \pi_j \tau_{ijk}$, $\alpha := n_i \pi_j Q_{ij}$, $\delta(\mathbf{x})$ being the Dirac delta function and π_i is the Cartesian component of the unit tangent vector on Γ.

Preprints (www.preprints.org) | NOT PEER-REVIEWED | Posted: 6 May 2020 doi:10.20944/preprints202005.0095.v1

Peer-reviewed version available at Materials 2020, 13, 2527; doi:10.3390/ma13112527

The jump at a corner ($\mathbf{x}^c$) on the oriented boundary contour Γ is defined as

$$\left\|\rho_i(\mathbf{x}^c)\right\| := \rho_i(\mathbf{x}^c - 0) - \rho_i(\mathbf{x}^c + 0), \tag{21}$$

$$\left\|\alpha(\mathbf{x}^c)\right\| := \alpha(\mathbf{x}^c - 0) - \alpha(\mathbf{x}^c + 0). \tag{22}$$

2.2 The MLPG formulation

The presence of gradients of strains and electric intensity vector in the electric enthalpy requires C^1 continuous interpolations of primary fields, i.e. displacements and electric potential. Recently, the mixed FEM has been developed for considered electro-elasticity problem [32]. The Meshless Local Petrov-Galerkin method (MLPG) with the Moving Least-square (MLS) approximation is convenient approach for problems with higher order derivatives, since the order of continuity can be tuned to a desired value [22-24].

The MLPG method is based on the local weak-form with local fictitious subdomains Ω^q constructed for each node $\mathbf{x}^q$ inside the analysed domain. The geometry of this subdomain can be arbitrary. However, it is appropriate to select a circular shape for simple numerical evaluation of integrals. One can write the local weak-form of the first governing equation (15) as

$$\int_{\Omega^q} \left[\sigma_{ij,j}(\mathbf{x}) - \tau_{ijk,jk}(\mathbf{x})\right] u^*_{im}(\mathbf{x})\, d\Omega = 0, \tag{23}$$

where $u^*_{im}(\mathbf{x})$ is a test function.

Applying the Gauss divergence theorem to domain integrals in (23) one can write

$$\int_{\partial\Omega^q} \left[\sigma_{ij}(\mathbf{x}) - \tau_{ijk,k}(\mathbf{x})\right] n_j(\mathbf{x}) u^*_{im}(\mathbf{x}) d\Gamma - \int_{\Omega^q} \left[\sigma_{ij}(\mathbf{x}) - \tau_{ijk,k}(\mathbf{x})\right] u^*_{im,j}(\mathbf{x}) d\Omega = 0, \tag{24}$$

where $\partial\Omega^q$ is the boundary of the local subdomain which consists of three parts $\partial\Omega^q = L^q \cup \Gamma^q_t \cup \Gamma^q_u$, in general (see Fig. 1).

If a Heaviside step function is chosen for the test function $u^*_{ik}(\mathbf{x})$ in each subdomain as

$$u^*_{ik}(\mathbf{x}) = \begin{cases} \delta_{ik} & \text{at } \mathbf{x} \in \Omega^q \cup \partial\Omega^q \\ 0 & \text{at } \mathbf{x} \notin \Omega^q \cup \partial\Omega^q \end{cases}, \tag{25}$$

the local weak-form (24) is transformed into the local integral equation

$$\int_{L^q + \Gamma^q_u} n_j \left(\sigma_{ij} - \tau_{ijk,k}\right) d\Gamma + \rho_i(\mathbf{x}^f_t) - \rho_i(\mathbf{x}^s_t) = -\int_{\Gamma^q_t} \bar{t}_i d\Gamma, \tag{26}$$

where $\mathbf{x}^f_t$, $\mathbf{x}^s_t$ stand for the final and starting points on Γ^q_t.

Preprints (www.preprints.org) | NOT PEER-REVIEWED | Posted: 6 May 2020 doi:10.20944/preprints202005.0095.v1

Peer-reviewed version available at Materials 2020, 13, 2527; doi:10.3390/ma13112527

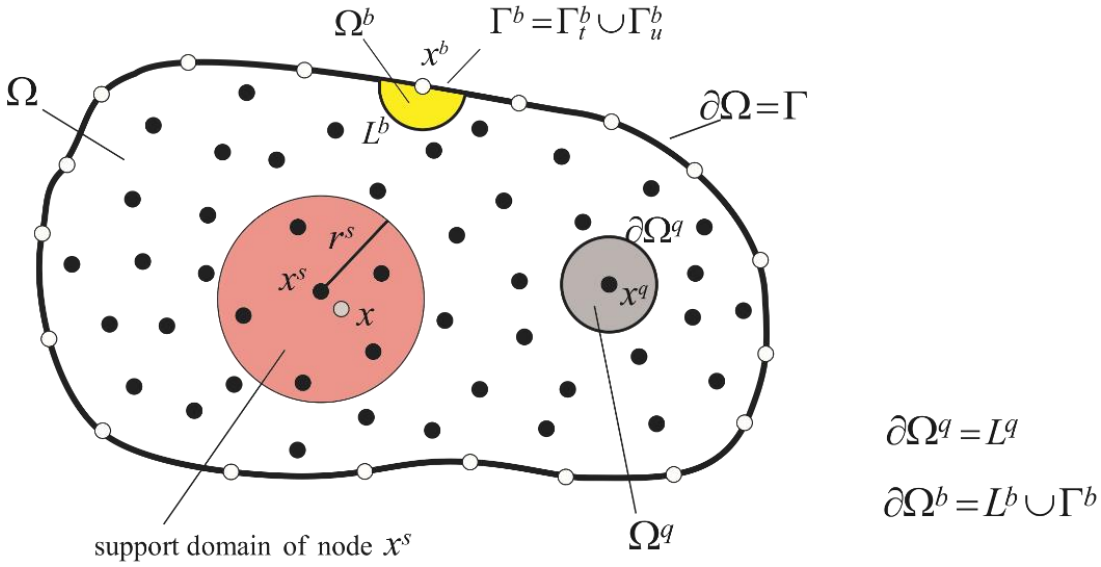

Fig. 1: Local subdomains Ω^q and Ω^b with their boundaries for MLS approximation of the trial function; support domain of weight function around node $\mathbf{x}^s$

Similarly, we get local integral equation for the second governing equation (15)

$$\int_{L^q+\Gamma_\phi^q} n_j \left(D_j - Q_{ij,i}\right) d\Gamma + \alpha(\mathbf{x}_S^f) - \alpha(\mathbf{x}_S^s) = -\int_{\Gamma_S^q} \bar{S} d\Gamma \,. \tag{27}$$

For numerical solution of the above integral equations (26) and (27), the MLS approximation of trial functions is applied. The primary fields (mechanical displacements and electric potential) are given by [23]

$$\mathbf{u}^h(\mathbf{x}) = \mathbf{N}^T(\mathbf{x}) \cdot \hat{\mathbf{u}} = \sum_{a=1}^{n} N^a(\mathbf{x}) \hat{\mathbf{u}}^a, \qquad \phi^h(\mathbf{x}) = \sum_{a=1}^{n} N^a(\mathbf{x}) \hat{\phi}^a, \tag{28}$$

where $\hat{\mathbf{u}}^a = \left(\hat{u}_1^a, \hat{u}_3^a\right)^T$ and $\hat{\phi}^a$ are fictitious nodal parameters for displacements and electric potential, respectively, and $N^a(\mathbf{x})$ is the shape function related to the node a. The number of nodes, n, used for the approximation is determined by the size of support domain of the weight function $w^a(\mathbf{x})$. In standard discretization methods like the FEM, there are observed discontinuities on interfaces of elements if continuity of approximation is not sufficient. In meshless methods there are no element interfaces and we can use the forth-order spline-type weight function with C^1 – continuity even for our problem with derivatives of the third order. The weight function has the following form

$$w^a(\mathbf{x}) = \begin{cases} 1-6\left(\frac{d^a}{r^a}\right)^2+8\left(\frac{d^a}{r^a}\right)^3-3\left(\frac{d^a}{r^a}\right)^4, & 0 \le d^a \le r^a \\ 0, & d^a \ge r^a \end{cases}, \tag{29}$$

where $d^a = \left\|\mathbf{x}-\mathbf{x}^a\right\|$, and r^a is the size of the support domain.

The strains and electric intensity vector is approximated by

$$\boldsymbol{\varepsilon}^h(\mathbf{x}) = \begin{bmatrix} \varepsilon^h_{11} \\ \varepsilon^h_{33} \\ 2\varepsilon^h_{13} \end{bmatrix} = \sum_{a=1}^{n} \mathbf{B}^a(\mathbf{x})\hat{\mathbf{u}}^a, \quad \mathbf{E}^h(\mathbf{x}) = \begin{bmatrix} E^h_1 \\ E^h_3 \end{bmatrix} = -\sum_{a=1}^{n} \mathbf{P}^a(\mathbf{x})\hat{\phi}^a,$$

$$\boldsymbol{\varepsilon}^h_{,k}(\mathbf{x}) = \begin{bmatrix} \varepsilon^h_{11,k} \\ \varepsilon^h_{33,k} \\ 2\varepsilon^h_{13,k} \end{bmatrix} = \sum_{a=1}^{n} \mathbf{B}^a_{,k}(\mathbf{x})\hat{\mathbf{u}}^a, \quad \mathbf{E}^h_{,k}(\mathbf{x}) = \begin{bmatrix} E^h_{1,k} \\ E^h_{3,k} \end{bmatrix} = -\sum_{a=1}^{n} \mathbf{P}^a_{,k}(\mathbf{x})\hat{\phi}^a \tag{30}$$

where

$$\mathbf{B}^a(\mathbf{x}) = \begin{bmatrix} N^a_{,1} & 0 \\ 0 & N^a_{,3} \\ N^a_{,3} & N^a_{,1} \end{bmatrix}, \quad \mathbf{P}^a(\mathbf{x}) = \begin{bmatrix} N^a_{,1} \\ N^a_{,3} \end{bmatrix}, \quad \mathbf{B}^a_{,k}(\mathbf{x}) = \begin{bmatrix} N^a_{,1k} & 0 \\ 0 & N^a_{,3k} \\ N^a_{,3k} & N^a_{,1k} \end{bmatrix}, \quad \mathbf{P}^a_{,k}(\mathbf{x}) = \begin{bmatrix} N^a_{,1k} \\ N^a_{,3k} \end{bmatrix}. \tag{31}$$

The first part of the traction vector (19), $\tilde{t}_i(\mathbf{x}) = n_j(\sigma_{ij} - \tau_{ijk,k})$, can be approximated at a boundary point $\mathbf{x} \in \partial\Omega^b$ in terms of primary fields as

$$\tilde{\mathbf{t}}^h(\mathbf{x}) = \boldsymbol{\mathcal{N}}(\mathbf{x})\mathbf{C}\sum_{a=1}^{n}\left(\mathbf{B}^a(\mathbf{x}) - l^2\mathbf{B}^a_{,kk}(\mathbf{x})\right)\hat{\mathbf{u}}^a + \boldsymbol{\mathcal{N}}(\mathbf{x})\sum_{a=1}^{n}\left(\boldsymbol{\Lambda}\mathbf{P}^a(\mathbf{x}) + \boldsymbol{\Phi}_k\mathbf{P}^a_{,k}(\mathbf{x}) - \mathbf{F}^T_k\mathbf{P}^a_{,k}(\mathbf{x})\right)\hat{\phi}^a \quad , \tag{32}$$

where the matrices $\mathbf{C}$, $\boldsymbol{\Lambda}, \boldsymbol{\Phi}_k, \mathbf{F}^T_k$ are defined in eq. (11) and (13), and the matrix $\boldsymbol{\mathcal{N}}(\mathbf{x})$ is related to the normal vector $\mathbf{n}(\mathbf{x})$ on $\partial\Omega^b$ by

$$\boldsymbol{\mathcal{N}}(\mathbf{x}) = \begin{bmatrix} n_1 & 0 & n_3 \\ 0 & n_3 & n_1 \end{bmatrix}. \tag{33}$$

Again the first part of the electric charge (27), $\tilde{S}(\mathbf{x}) = n_j(D_j - Q_{ij,i})$, has to be approximated. In the first step the expression of $Q_{ij,i}$ is given by

$$n_j Q_{ij,i} = n_j\begin{bmatrix}\partial_1 & \partial_3\end{bmatrix}\begin{bmatrix} Q_{1j} \\ Q_{3j} \end{bmatrix} = n_j\begin{bmatrix}\partial_1 & \partial_3\end{bmatrix}\left\{\boldsymbol{\Phi}^T_j\sum_{a=1}^{n}\mathbf{B}^a(\mathbf{x})\hat{\mathbf{u}}^a - q^2\mathbf{A}\sum_{a=1}^{n}\mathbf{P}^a_{,j}(\mathbf{x})\hat{\phi}^a\right\} =$$

$$= n_j(\mathbf{x})\left\{\sum_{a=1}^{n}\boldsymbol{\Psi}^a_j(\mathbf{x})\hat{\mathbf{u}}^a - q^2\sum_{a=1}^{n}\boldsymbol{\Pi}^a_j(\mathbf{x})\hat{\phi}^a\right\}, \tag{34}$$

Preprints (www.preprints.org) | NOT PEER-REVIEWED | Posted: 6 May 2020 doi:10.20944/preprints202005.0095.v1

Peer-reviewed version available at Materials 2020, 13, 2527; doi:10.3390/ma13112527

where,

$$\boldsymbol{\Psi}_1^{aT}(\mathbf{x})=\begin{bmatrix} b_1N^a_{,11}+b_3N^a_{,33} \\ (b_1+b_3)N^a_{,13}\end{bmatrix},\qquad \boldsymbol{\Psi}_3^{aT}(\mathbf{x})=\begin{bmatrix} (b_1+b_2)N^a_{,13} \\ b_2N^a_{,11}+b_1N^a_{,33}\end{bmatrix},\qquad \boldsymbol{\Pi}_j^{a}(\mathbf{x})=\begin{bmatrix} a_1N^a_{,11j} \\ a_2N^a_{,33j}\end{bmatrix}.$$

Now, $\tilde{S}(\mathbf{x})$ can be approximated by

$$\begin{aligned}\tilde{S}^h(\mathbf{x})=\mathbf{N}(\mathbf{x})\left\{\sum_{a=1}^{n}\left(\boldsymbol{\Lambda}^T\mathbf{B}^a(\mathbf{x})+\mathbf{F}_k\mathbf{B}^a_{,k}(\mathbf{x})\right)\hat{\mathbf{u}}^a-\mathbf{A}\sum_{a=1}^{n}\mathbf{P}^a(\mathbf{x})\hat{\phi}^a\right\}-\\ -n_j(\mathbf{x})\left\{\sum_{a=1}^{n}\boldsymbol{\Psi}^a_j(\mathbf{x})\hat{\mathbf{u}}^a-q^2\sum_{a=1}^{n}\boldsymbol{\Pi}^a_j(\mathbf{x})\hat{\phi}^a\right\}\end{aligned}, \tag{35}$$

with $\mathbf{N}(\mathbf{x})=\begin{bmatrix} n_1(\mathbf{x}) & n_3(\mathbf{x})\end{bmatrix}$.

The essential boundary conditions are satisfied in the strong-form at nodal points $\zeta^b\in\left(\Gamma^b_u\cup\Gamma^b_s\cup\Gamma^b_\phi\cup\Gamma^b_p\right)\subset\partial\Omega$. If the approximation formulas (28) and (30) are used one can write

$$\begin{aligned}&\sum_{a=1}^{n}N^a(\zeta^b)\hat{\mathbf{u}}^a=\bar{\mathbf{u}}(\zeta^b)\quad \text{for } \zeta^b\in\Gamma^b_u, && \mathbf{N}(\zeta^b)\sum_{a=1}^{n}\mathbf{P}^a(\zeta^b)\hat{\mathbf{u}}^a=\bar{\mathbf{s}}(\zeta^b)\quad \text{for } \zeta^b\in\Gamma^b_s\\ &\sum_{a=1}^{n}N^a(\zeta^b)\hat{\phi}^a=\bar{\phi}(\zeta^b)\quad \text{for } \zeta^b\in\Gamma^b_\phi, && \mathbf{N}(\zeta^b)\sum_{a=1}^{n}\mathbf{P}^a(\zeta^b)\hat{\phi}^a=\bar{p}(\zeta^b)\quad \text{for } \zeta^b\in\Gamma^b_p\end{aligned}. \tag{36}$$

Substituting the MLS-approximation (32) and (35) into the local boundary-domain integral equations (26) and (27), we obtain the system of algebraic equations for unknown nodal quantities

$$\begin{aligned}&\int_{L^q+\Gamma^q_u}\mathcal{N}(\mathbf{x})\mathbf{C}\sum_a\left(\mathbf{B}^a(\mathbf{x})-l^2\mathbf{B}^a_{,kk}(\mathbf{x})\right)\hat{\mathbf{u}}^a d\Gamma(\mathbf{x})+\\ &+\int_{L^q+\Gamma^q_u}\mathcal{N}(\mathbf{x})\sum_{a=1}^{n}\left(\boldsymbol{\Lambda}\mathbf{P}^a(\mathbf{x})+\boldsymbol{\Phi}_k\mathbf{P}^a_{,k}(\mathbf{x})-\mathbf{F}_k^T\mathbf{P}^a_{,k}(\mathbf{x})\right)\hat{\phi}^a d\Gamma(\mathbf{x})+\\ &+n_k(\mathbf{x}^f_t)\boldsymbol{\Pi}(\mathbf{x}^f_t)\left(l^2\mathbf{C}\sum_a\mathbf{B}^a_{,k}(\mathbf{x}^f_t)\hat{\mathbf{u}}^a+\mathbf{F}_k^T\sum_a\mathbf{P}^a(\mathbf{x}^f_t)\hat{\phi}^a\right)-\\ &-n_k(\mathbf{x}^s_t)\boldsymbol{\Pi}(\mathbf{x}^s_t)\left(l^2\mathbf{C}\sum_a\mathbf{B}^a_{,k}(\mathbf{x}^s_t)\hat{\mathbf{u}}^a+\mathbf{F}_k^T\sum_a\mathbf{P}^a(\mathbf{x}^s_t)\hat{\phi}^a\right)=-\int_{\Gamma^q_t}\bar{\mathbf{t}}(\mathbf{x})d\Gamma\end{aligned}, \tag{37}$$

Preprints (www.preprints.org) | NOT PEER-REVIEWED | Posted: 6 May 2020 doi:10.20944/preprints202005.0095.v1

Peer-reviewed version available at Materials 2020, 13, 2527; doi:10.3390/ma13112527

$$\int_{L^q+\Gamma_\phi^q} \mathbf{N}(\mathbf{x})\left[\sum_{a=1}^{n}\left(\mathbf{\Lambda}^T\mathbf{B}^a(\mathbf{x})+\mathbf{F}_k\mathbf{B}^a_{,k}(\mathbf{x})\right)\hat{\mathbf{u}}^a-\mathbf{A}\sum_{a=1}^{n}\mathbf{P}^a(\mathbf{x})\hat{\phi}^a\right]d\Gamma(\mathbf{x})-$$
$$-\int_{L^q+\Gamma_\phi^q} n_j(\mathbf{x})\left[\sum_{a=1}^{n}\mathbf{\Psi}^a_j(\mathbf{x})\hat{\mathbf{u}}^a-q^2\sum_{a=1}^{n}\mathbf{\Pi}^a_j(\mathbf{x})\hat{\phi}^a\right]d\Gamma(\mathbf{x})+$$
$$+\mathbf{N}(\mathbf{x}_S^f)\pi_k(\mathbf{x}_S^f)\left(\mathbf{\Phi}_k^T\sum_a\mathbf{B}^a(\mathbf{x}_S^f)\hat{\mathbf{u}}^a-q^2\mathbf{A}\sum_a\mathbf{P}^a_{,k}(\mathbf{x}_S^f)\hat{\phi}^a\right)$$
$$-\mathbf{N}(\mathbf{x}_S^s)\pi_k(\mathbf{x}_S^s)\left(\mathbf{\Phi}_k^T\sum_a\mathbf{B}^a(\mathbf{x}_S^s)\hat{\mathbf{u}}^a-q^2\mathbf{A}\sum_a\mathbf{P}^a_{,k}(\mathbf{x}_S^s)\hat{\phi}^a\right)=-\int_{\Gamma_S^q}\bar{S}(\mathbf{x})d\Gamma \quad , \tag{38}$$

which are considered on the sub-domains adjacent to the interior nodes $x^q \in \Omega$ as well as to the boundary nodes on $x^q \in \Gamma_t^q \subset \partial\Omega$ and/or $x^q \in \Gamma_S^q \subset \partial\Omega$ with

$$\mathbf{\Pi}(\mathbf{x})=\begin{bmatrix}\pi_1(\mathbf{x}) & 0 & \pi_3(\mathbf{x})\\ 0 & \pi_3(\mathbf{x}) & \pi_1(\mathbf{x})\end{bmatrix} \quad . \tag{39}$$

2.3 Numerical examples

A square panel under bending in Fig. 2 is analyzed by the FEM [31] and the MLPG. The piezoelectric material PZT-5H is chosen for the study.

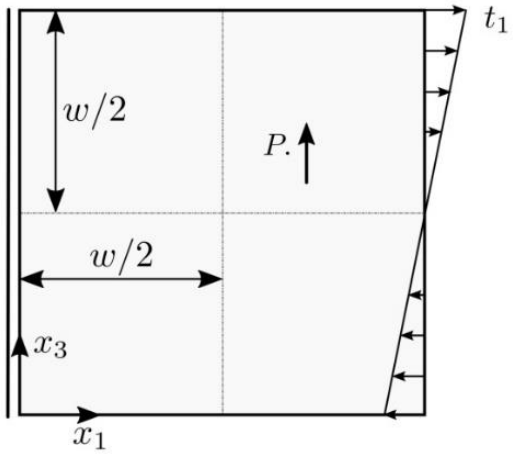

Fig. 2: A square piezoelectric panel under bending

Polarization of material is considered along x_3 coordinate. Following geometry and load are considered in numerical analysis: $w=1.0\times10^{-7}\text{m}$, $t_1=1.0\times10^{6}\text{MPa}$. The size effect is control by parameter α, defined by $l^2=\alpha l_0^2$ with micro-length scale parameter $l_0=5\times10^{-9}\text{m}$. The flexoelectric coefficients are vanishing here.

Preprints (www.preprints.org) | NOT PEER-REVIEWED | Posted: 6 May 2020 doi:10.20944/preprints202005.0095.v1

Peer-reviewed version available at Materials 2020, 13, 2527; doi:10.3390/ma13112527

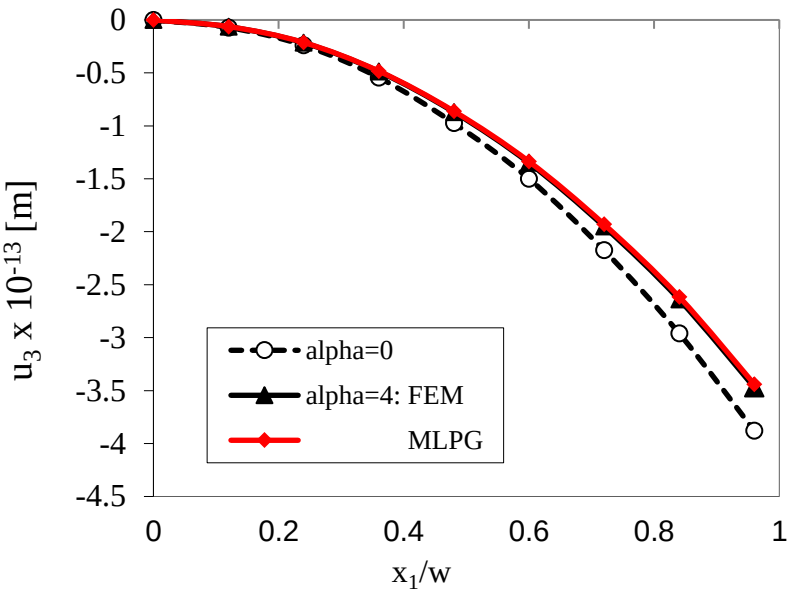

Fig. 3: Variation of the mechanical displacement u_3 at x_3=w/2

The variation of the panel deflection along x_1 is presented in Fig. 3. Results are obtained by classical and gradient theories. In gradient theory only strain gradients are considered in constitutive equations. Gradients of electric intensity vector are vanishing. The deflections resulting from the gradient theory are reduced with respect to those obtained by the classical approach. The FEM and MLPG results are in a good agreement.

A square plate with a central crack with the geometrical parameters $w = 5a$, $a = 1.0\times10^{-7}$m is analyzed (see Fig. 4) in the next example. On the top and the bottom boundaries of the plate a combined electro-mechanical loading with $t_3 = 1.17$MPa and $D_3 = -5\times10^{-4}$C/m^2 is applied. The crack-faces are free of mechanical tractions and electrical displacements.

The flexoelectric coefficients are considered to be $f_1 = f_2 = f_0 = 1\times10^{-8}$C/m. The converse flexoelectric coefficients and length scale parameter for the higher-order electric parameters are selected as $b_1 = b_2 = b_3 = b_0 = 5\times10^{-8}$C/m and $q^2 = q_0^2 = 5\times10^{-10}$m^2, respectively. To assess the effects of the strain- and electric field-gradients, the size-factors l^2, b_i, q^2 and f in constitutive equations are defined by

$$l^2 = \alpha l_0^2 \,, \quad f_i = \alpha f_0 \,, \quad b_i = \beta b_0 \,, \quad q^2 = \beta q_0^2 \,.$$

To investigate influence of the strain gradient and electric intensity gradient parameters various integer numbers α and β are selected in numerical analyses.

Preprints (www.preprints.org) | NOT PEER-REVIEWED | Posted: 6 May 2020 doi:10.20944/preprints202005.0095.v1

Peer-reviewed version available at Materials 2020, 13, 2527; doi:10.3390/ma13112527

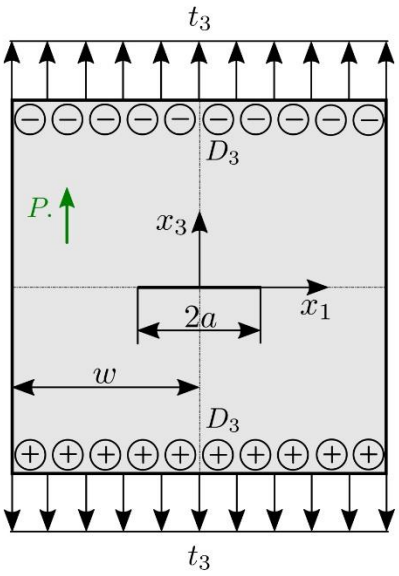

Fig. 4: Crack in a square plate under an electro-mechanical loading

Crack opening displacement and induced electric potential are presented in Fig. 5. One can observe that both displacement and electric potential are reduced if the converse flexoelectricity is growing (larger β).

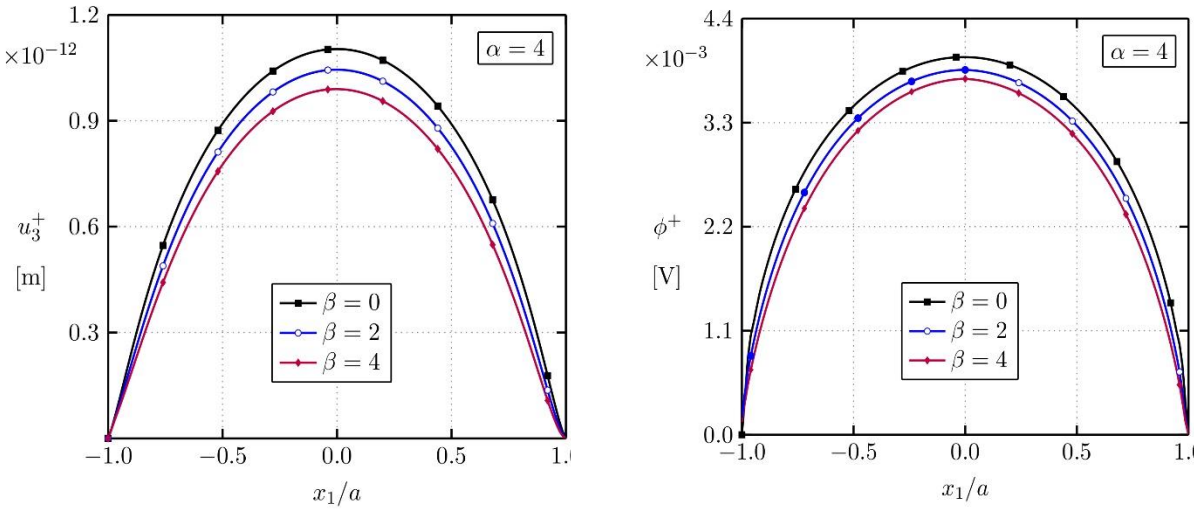

Fig. 5: Crack opening-displacements u_3^+ and electrical potentials ϕ^+ of the upper crack-face for different factors β

3 Gradient theory in thermoelectric materials

The thermoelectric conversion efficiency is high if the thermal conductivity is low. It can be reduced significantly in nano-sized structures. It is due to comparable sizes of phonon mean free path and the structure. Phonons are scattered on interfaces and thermal conductivity is reduced.

For this purpose it is needed to develop a theory of heat conduction, where size effect is considered. It is well known that there is no size effect considered in the classical local theory of Fourier heat conduction. Similarly to the elasticity problems in nanostructures it is possible to consider the size effect here through the nonlocal heat transport [19]. The heat flux vector in nonlocal theory is given by

$$\lambda_i(\mathbf{x}) = -\int_V \alpha(\mathbf{x}-\mathbf{y})\kappa_{ij}(\mathbf{y})\theta_{,j}(\mathbf{y})dV(\mathbf{y}) \ , \tag{40}$$

where the temperature differences are denoted by $\theta = T - T_0$ with the reference temperature T_0, κ_{ij} is the thermal conductivity and $\alpha(\mathbf{x}-\mathbf{y})$ is a nonlocal kernel function.

The nonlocal weight function can be selected as

$$\alpha = \frac{1}{4\pi l^2 \rho}\exp(-\rho / l) \ , \tag{41}$$

where $\rho = |\mathbf{x}-\mathbf{y}|$ distance and l is a characteristic length material parameter.

It is easy to show that weight function (41) satisfies the Helmholtz equation

$$\left(1-l^2\nabla^2\right)\alpha(|\mathbf{x}-\mathbf{y}| = \delta(\mathbf{x}-\mathbf{y}) \, , \tag{42}$$

where $\delta(\mathbf{x}-\mathbf{y})$ is the Dirac function.

Then, the integral expression (40) is reduced to the Helmholtz equation

$$\left(1-l^2\nabla^2\right)\lambda_i = -\kappa_{ij}\theta_{,j} \text{ or } \left(1-l^2\nabla^2\right)\lambda_{i,i} = w \tag{43}$$

where w is the volume density of heat source.

By this way it is possible to replace the integro-differential form of the constitutive law in (40) by a more convenient differential form given in (43). Then, higher order derivatives in the governing equation appear in this non-local theory of heat conduction than in the classical local Fourier theory.

Formally, the same governing equation as given in Eq. (43), can be obtained also in the higher-grade theory with including the higher-grade heat flux m_{ik} (i.e. canonically conjugated fields with $\theta_{,jk}$) into constitutive equations in addition to the classical heat flux λ_i as

$$\lambda_i = -\kappa_{ij}\theta_{,j} \ , \tag{44}$$

$$m_{ik} = -l^2\kappa_{ij}\theta_{,jk} \ . \tag{45}$$

The constitutive equations for thermoelectric materials with higher order heat conduction theory can be written as

$$\lambda_i = -\bar{\kappa}_{ij}\theta_{,j} + \bar{\zeta}_{ij}E_j ,$$

$$J_i = s_{ij}E_j - \zeta_{ij}\theta_{,j} ,$$

$$m_{ik} = -l^2\kappa_{ij}\theta_{,jk} \ , \tag{46}$$

where the electric current density is denoted by J_i and s_{ij} , ζ_{ij} , $\bar{\zeta}_{ij}$ are the electrical conductivity measured with keeping uniform temperature, Seebeck and Peltier coefficients, respectively. Note that the latter two coefficients are correlated via the absolute temperature T as $\bar{\zeta}_{ij} = \zeta_{ij}T$, with $T = T_0 + \theta$, where T_0 is the reference temperature. Furthermore, $\bar{\kappa}_{ij} = (\kappa_{ij} + \kappa^e_{ij})$ is composed of the heat conduction κ_{ij} measured when $J_i = 0$ and contribution to heat conduction κ^e_{ij} because of electric current [33]. The Seebeck coefficient is proportional to the electric current conductivity $\zeta_{ij} = \alpha s_{ij}$, $\bar{\zeta}_{ij} = \alpha s_{ij}T$ and $\bar{\kappa}_{ij} = (\kappa_{ij} + \alpha^2 s_{ij}T)$.

The electric intensity vector E_j is related to the electric potential ϕ by

$$E_j = -\phi_{,j} \ . \tag{47}$$

Next, orthotropic material properties are considered and the matrix form of constitutive equations (46) for 2-d problems are given by

$$\begin{pmatrix} J_1 \\ J_2 \end{pmatrix} = \begin{pmatrix} s_{11} & 0 \\ 0 & s_{22} \end{pmatrix}\begin{pmatrix} E_1 \\ E_2 \end{pmatrix} - \begin{pmatrix} \zeta_{11} & 0 \\ 0 & \zeta_{22} \end{pmatrix}\begin{pmatrix} \theta_{,1} \\ \theta_{,2} \end{pmatrix} = [\mathbf{S}]\{\mathbf{E}\} - [\mathbf{Z}]\begin{pmatrix} \theta_{,1} \\ \theta_{,2} \end{pmatrix} , \tag{48}$$

$$\begin{pmatrix} \lambda_1 \\ \lambda_2 \end{pmatrix} = \begin{pmatrix} \bar{\zeta}_{11} & 0 \\ 0 & \bar{\zeta}_{22} \end{pmatrix}\begin{pmatrix} E_1 \\ E_2 \end{pmatrix} - \begin{pmatrix} \bar{\kappa}_{11} & 0 \\ 0 & \bar{\kappa}_{22} \end{pmatrix}\begin{pmatrix} \theta_{,1} \\ \theta_{,2} \end{pmatrix} = [\bar{\mathbf{Z}}]\{\mathbf{E}\} - [\bar{\boldsymbol{\kappa}}]\begin{pmatrix} \theta_{,1} \\ \theta_{,2} \end{pmatrix}, \tag{49}$$

$$\begin{pmatrix} m_{1k} \\ m_{2k} \end{pmatrix} = -l^2\begin{pmatrix} \kappa_{11} & 0 \\ 0 & \kappa_{22} \end{pmatrix}\begin{pmatrix} \theta_{,1k} \\ \theta_{,2k} \end{pmatrix} = -l^2[\boldsymbol{\kappa}]\begin{pmatrix} \theta_{,1k} \\ \theta_{,2k} \end{pmatrix}. \tag{50}$$

Then, the governing equations for stationary thermoelectric problem are given by conservation of energy and electric charge as

$$\lambda_{i,i} - m_{ik,ik} = w$$

$$J_{i,i} = 0 \ . \tag{51}$$

The weak form of these equations can be written as

$$\begin{aligned}
&\int_V \left(J_i \delta\phi_{,i} + \lambda_i \delta\theta_{,i} + m_{ik} \delta\theta_{,ik} \right) dV + \int_V w \delta\theta dV = \\
&\quad = -\int_V \left[J_{i,i} \delta\phi + \left(\lambda_{i,i} - w \right) \delta\theta + m_{ik,k} \delta\theta_{,i} \right] dV + \\
&\quad + \int_{\partial V} \left(n_i J_i \delta\phi + n_i \lambda_i \delta\theta + n_k m_{ik} \delta\theta_{,i} \right) d\Gamma = \\
&\quad - \int_V \left[J_{i,i} \delta\phi + \left(\lambda_{i,i} - m_{ik,ik} - w \right) \delta\theta \right] dV + \\
&\quad + \int_{\partial V} \left[n_i J_i \delta\phi + n_i \left(\lambda_i - m_{ik,k} \right) \delta\theta + n_k m_{ik} \delta\theta_{,i} \right] d\Gamma = \\
&\quad = -\int_V \left[J_{i,i} \delta\phi + \left(\lambda_{i,i} - m_{ik,ik} - w \right) \delta\theta \right] dV - \\
&\quad - \int_{\partial V} \left(\Lambda \delta\theta + P \delta p + Q \delta\phi \right) d\Gamma
\end{aligned} \tag{52}$$

where P, Q and Λ are independent boundary densities conjugated with $p = \partial\theta / \partial \mathbf{n}$, ϕ and θ, respectively, and given as $P = n_k n_i m_{ik}$, $Q = n_k J_k$

$$\Lambda = n_j \left(\lambda_i - m_{ik,k} \right) - \frac{\partial \mu}{\partial \boldsymbol{\pi}} + \sum_c \left[\!\left[\mu(\mathbf{x}^c) \right]\!\right] \delta(\mathbf{x} - \mathbf{x}^c) \tag{53}$$

$$\mu = n_k \pi_i m_{ik} \tag{54}$$

with Λ being the heat flux, n_i and π_i are the Cartesian component of the unit tangent vector on Γ, and the jump at a corner on the oriented boundary contour Γ is defined as $\left[\!\left[\mu(\mathbf{x}^c) \right]\!\right] := \mu(\mathbf{x}^c - 0) - \mu(\mathbf{x}^c + 0)$.

The rate of work of the external "forces" $\left(\bar{\Lambda}, \bar{P}, \bar{Q} \right)$ and body source is given by

$$\delta W = \int_{\Gamma_\Lambda} \bar{\Lambda} \delta\theta d\Gamma + \int_{\Gamma_P} \bar{P} \delta p d\Gamma + \int_{\Gamma_Q} \bar{Q} \delta\phi d\Gamma + \int_V w \delta\theta dV . \tag{55}$$

If only the Joule heating plays the role of heat sources,

$$\delta W = \int_{\Gamma_\Lambda} \bar{\Lambda} \delta\theta d\Gamma + \int_{\Gamma_P} \bar{P} \delta p d\Gamma + \int_{\Gamma_Q} \bar{Q} \delta\phi d\Gamma + \int_V E_i J_i \delta\theta dV \quad , \tag{56}$$

and the governing equations become

$$\lambda_{i,i}(\mathbf{x}) - m_{ik,ik}(\mathbf{x}) - E_i(\mathbf{x}) J_i(\mathbf{x}) = 0 , \quad J_{i,i}(\mathbf{x}) = 0 . \tag{57}$$

Furthermore, from the weak formulation, one can deduce the following boundary conditions for coupled thermoelectric problem considered within higher-grade theory

essential b.c.: $\theta(\mathbf{x}) = \bar{\theta}(\mathbf{x})$ on Γ_θ , $\Gamma_\theta \subset \Gamma$

$p(\mathbf{x}) = \bar{p}(\mathbf{x})$ on Γ_p , $\Gamma_p \subset \Gamma$

$$\phi(\mathbf{x}) = \bar{\phi}(\mathbf{x}) \text{ on } \Gamma_\phi \ , \ \Gamma_\phi \subset \Gamma$$

natural b.c: $\Lambda(\mathbf{x}) = \bar{\Lambda}(\mathbf{x})$ on Γ_Λ , $\Gamma_\Lambda \cup \Gamma_\theta = \Gamma$, $\Gamma_\Lambda \cap \Gamma_\theta = \varnothing$

$$P(\mathbf{x}) = \bar{P}(\mathbf{x}) \text{ on } \Gamma_P \ , \ \Gamma_P \cup \Gamma_p = \Gamma \ , \ \Gamma_P \cap \Gamma_p = \varnothing$$

$$Q(\mathbf{x}) = \bar{Q}(\mathbf{x}) \text{ on } \Gamma_Q \ , \ \Gamma_Q \cup \Gamma_\phi = \Gamma \ , \ \Gamma_Q \cap \Gamma_\phi = \varnothing \ .$$

Substituting the constitutive relationships into the governing equations, we obtain the non-linear system of the PDEs for primary field variables θ and ϕ

$$\kappa_{ij}\left(1-l^2\nabla^2\right)\theta_{,ij} + \zeta_{ij}T\left(\phi_{,ij}+\alpha\theta_{,ij}\right) + \zeta_{ij}\theta_{,i}\left(\phi_{,j}+\alpha\theta_{,j}\right) + \phi_{,i}\left(s_{ij}\phi_{,j}+\zeta_{ij}\theta_{,j}\right) = 0 \ ,$$

$$s_{ij}\phi_{,ij} + \zeta_{ij}\theta_{,ij} = 0 \ .$$

Recall that owing to the Joule heat, the problem is non-linear even if the temperature dependence of material coefficients were neglected. Finally, making use the proportionality relationship $\zeta_{ij} = \alpha s_{ij}$, the system of governing equations become

$$\kappa_{ij}\left(1-l^2\nabla^2\right)\theta_{,ij} + s_{ij}\left(\phi_{,i}+\alpha\theta_{,i}\right)\left(\phi_{,j}+\alpha\theta_{,j}\right) = 0 \ ,$$

$$s_{ij}\left(\phi_{,ij}+\alpha\theta_{,ij}\right) = 0 \ .$$

3.1 The MLPG formulation in thermoelectricity

One can see in the previous chapter that MLPG method is based on the local weak-form with local fictitious subdomains Ω^q . The local weak-form of the first governing equation (57) is given as

$$\int_{\Omega^q}\left[\lambda_{i,i}(\mathbf{x}) - m_{ik,ik}(\mathbf{x}) - E_i J_i\right] u^*(\mathbf{x})\, d\Omega \ = 0 \ , \tag{58}$$

where $u^*(\mathbf{x})$ is a test function.

Applying the Gauss divergence theorem to two domain integrals in (58), one can write

$$\int_{\partial\Omega^q}\left[\lambda_i(\mathbf{x}) - m_{ik,k}(\mathbf{x})\right] n_i(\mathbf{x}) u^*(\mathbf{x}) d\Gamma - \int_{\Omega^q}\left[\lambda_i(\mathbf{x}) - m_{ik,k}(\mathbf{x})\right] u^*_{,i}(\mathbf{x}) d\Omega -$$

$$- \int_{\Omega^q} E_i(\mathbf{x}) J_i(\mathbf{x}) u^*(\mathbf{x}) d\Omega = 0 \ , \tag{59}$$

where $\partial\Omega^q$ is the boundary of the local subdomain Ω^q .

The test function can be arbitrary and we have selected a Heaviside step function

$$u^*(\mathbf{x}) = \begin{cases} 1 & \text{at} \quad \mathbf{x} \in \Omega^q \cup \partial\Omega^q \\ 0 & \text{at} \quad \mathbf{x} \notin \Omega^q \cup \partial\Omega^q \end{cases}. \tag{60}$$

Then, the local weak-form (59) is transformed into the local integral equation

$$\int_{L^q+\Gamma_\theta^q} n_i \left(\lambda_i - m_{ik,k}\right) d\Gamma + \mu(\mathbf{x}_\Lambda^f) - \mu(\mathbf{x}_\Lambda^s) - \int_{\Omega^q} E_i J_i \, d\Omega = -\int_{\Gamma_\Lambda^q} \bar{\Lambda} d\Gamma, \tag{61}$$

where $\mathbf{x}_\Lambda^f$, $\mathbf{x}_\Lambda^s$ stand for the final and starting points on Γ_Λ^q with prescribed heat flux.

The local integral equation for the second governing equation (57) is given as

$$\int_{L^q+\Gamma_\phi^q} n_i J_i d\Gamma = -\int_{\Gamma_Q^q} \bar{Q} d\Gamma. \tag{62}$$

The MLS approximation of trial functions is applied for numerical solution of the above local integral equations (61) and (62). The temperature and electric potential are approximated by [23]

$$\theta^h(\mathbf{x}) = \sum_{a=1}^{n} N^a(\mathbf{x})\hat{\theta}^a, \qquad \phi^h(\mathbf{x}) = \sum_{a=1}^{n} N^a(\mathbf{x})\hat{\phi}^a, \tag{63}$$

where $\hat{\theta}^a$ and $\hat{\phi}^a$ are fictitious nodal parameters for temperature and electric potential, respectively, and $N^a(\mathbf{x})$ is the shape function related to the node *a*. The number of nodes *n* is explained in Sect 2.2.

From the definition of heat flux λ_i and the higher-grade heat flux m_{ik} in (44), (45) and approximation of temperature (63) we get

$$\boldsymbol{\lambda}^h(\mathbf{x}) = \begin{pmatrix} \lambda_1 \\ \lambda_2 \end{pmatrix}^h = -\bar{\boldsymbol{\kappa}} \sum_{a=1}^{n} \mathbf{P}^a(\mathbf{x})\hat{\theta}^a - \bar{\mathbf{Z}} \sum_{a=1}^{n} \mathbf{P}^a(\mathbf{x})\hat{\phi}^a, \qquad \mathbf{m}_k^h(\mathbf{x}) = -l^2 \boldsymbol{\kappa} \sum_{a=1}^{n} \mathbf{P}_{,k}^a(\mathbf{x})\hat{\theta}^a \quad , \tag{64}$$

where

$$\mathbf{P}^a(\mathbf{x}) = \begin{bmatrix} N_{,1}^a \\ N_{,2}^a \end{bmatrix} \quad , \quad \mathbf{P}_{,k}^a(\mathbf{x}) = \begin{bmatrix} N_{,1k}^a \\ N_{,2k}^a \end{bmatrix}. \tag{65}$$

The electric current density and intensity of electric field are approximated by

$$\mathbf{J}^h(\mathbf{x}) = -\mathbf{S} \sum_{a=1}^{n} \mathbf{P}^a(\mathbf{x})\hat{\phi}^a - \mathbf{Z} \sum_{a=1}^{n} \mathbf{P}^a(\mathbf{x})\hat{\theta}^a, \qquad \mathbf{E}^T = -\sum_{c=1}^{n} \mathbf{P}^{cT}(\mathbf{x})\hat{\theta}^c \quad . \tag{66}$$

The incomplete heat flux $n_i(\lambda_i - m_{ik,k})$ and $\mu = n_k \pi_i m_{ik}$ are approximated as

Preprints (www.preprints.org) | NOT PEER-REVIEWED | Posted: 6 May 2020 doi:10.20944/preprints202005.0095.v1

Peer-reviewed version available at Materials 2020, 13, 2527; doi:10.3390/ma13112527

$$n_i(\lambda_i - m_{ik,k}) \approx \left(l^2 \mathbf{F}_\theta(\mathbf{x}) \sum_{a=1}^{n} \mathbf{P}^a_{,kk}(\mathbf{x}) - \bar{\mathbf{F}}_\theta(\mathbf{x}) \sum_{a=1}^{n} \mathbf{P}^a(\mathbf{x}) \right) \hat{\theta}^a - \bar{\mathbf{F}}_\phi(\mathbf{x}) \sum_{a=1}^{n} \mathbf{P}^a(\mathbf{x}) \hat{\phi}^a ,$$

$$\mu \approx -l^2 n_k(\mathbf{x}) \mathbf{F}_\mu(\mathbf{x}) \sum_{a=1}^{n} \mathbf{P}^a_{,k}(\mathbf{x}) \hat{\theta}^a , \tag{67}$$

where

$$\mathbf{F}_\theta(\mathbf{x}) = \left[n_1(\mathbf{x}) \quad n_2(\mathbf{x}) \right] \left[\boldsymbol{\kappa} \right] = \left[n_1(\mathbf{x}) \kappa_{11} \quad n_2(\mathbf{x}) \kappa_{22} \right],$$

$$\bar{\mathbf{F}}_\theta(\mathbf{x}) = \left[n_1(\mathbf{x}) \quad n_2(\mathbf{x}) \right] \left[\bar{\boldsymbol{\kappa}}(\mathbf{x}) \right] = \left[n_1(\mathbf{x}) \bar{\kappa}_{11}(\mathbf{x}) \quad n_2(\mathbf{x}) \bar{\kappa}_{22}(\mathbf{x}) \right],$$

$$\bar{\mathbf{F}}_\phi(\mathbf{x}) = \left[n_1(\mathbf{x}) \quad n_2(\mathbf{x}) \right] \left[\bar{\mathbf{Z}}(\mathbf{x}) \right] = \left[n_1(\mathbf{x}) \bar{\zeta}_{11}(\mathbf{x}) \quad n_2(\mathbf{x}) \bar{\zeta}_{22}(\mathbf{x}) \right],$$

$$\mathbf{F}_\mu(\mathbf{x}) = \left[\pi_1(\mathbf{x}) \quad \pi_2(\mathbf{x}) \right] \left[\boldsymbol{\kappa} \right] = \left[\pi_1(\mathbf{x}) \kappa_{11} \quad \pi_2(\mathbf{x}) \kappa_{22} \right],$$

with $\bar{\kappa}_{ij}(\mathbf{x}) = \left(\kappa_{ij} + \alpha^2 s_{ij}(T_0 + \theta(\mathbf{x})) \right)$, $\bar{\zeta}_{ij}(\mathbf{x}) = \zeta_{ij}\left(T_0 + \theta(\mathbf{x}) \right)$.

The essential boundary conditions are satisfied in the strong-form at nodal points $\zeta^b \in \left(\Gamma^b_\theta \cup \Gamma^b_p \cup \Gamma^b_\phi \right) \subset \partial\Omega$. These conditions follows directly from equations (63)

$$\sum_{a=1}^{n} N^a(\zeta^b) \hat{\theta}^a = \bar{\theta}(\zeta^b) \quad \text{for } \zeta^b \in \Gamma_\theta \text{ , } \mathbf{N}(\zeta^b) \sum_{a=1}^{n} \mathbf{P}^a(\zeta^b) \hat{\theta}^a = \bar{p}(\zeta^b) \quad \text{for } \zeta^b \in \Gamma_p ,$$

$$\sum_{a=1}^{n} N^a(\zeta^b) \hat{\phi}^a = \bar{\phi}(\zeta^b) \quad \text{for } \zeta^b \in \Gamma_\phi , \tag{68}$$

where $\mathbf{N}(\mathbf{x}) = \left[n_1(\mathbf{x}) \quad n_2(\mathbf{x}) \right]$.

Substituting the MLS-approximation (64) - (67) into the local boundary-domain integral equations (61) and (62), we obtain the nonlinear system of algebraic equations

$$\begin{aligned} \int_{L^q + \Gamma^q_\theta} & \left[\left(l^2 \mathbf{F}_\theta(\mathbf{x}) \sum_{a=1}^{n} \mathbf{P}^a_{,kk}(\mathbf{x}) - \bar{\mathbf{F}}_\theta(\mathbf{x}) \sum_{a=1}^{n} \mathbf{P}^a(\mathbf{x}) \right) \hat{\theta}^a - \bar{\mathbf{F}}_\phi(\mathbf{x}) \sum_{a=1}^{n} \mathbf{P}^a(\mathbf{x}) \hat{\phi}^a \right] d\Gamma + \\ & + l^2 \left(n_k(\mathbf{x}^s_\Lambda) \mathbf{F}_\mu(\mathbf{x}^s_\Lambda) \sum_{a=1}^{n} \mathbf{P}^a_{,k}(\mathbf{x}^s_\Lambda) - n_k(\mathbf{x}^f_\Lambda) \mathbf{F}_\mu(\mathbf{x}^f_\Lambda) \sum_{a=1}^{n} \mathbf{P}^a_{,k}(\mathbf{x}^f_\Lambda) \right) \hat{\theta}^a - \quad , \\ & - \int_{\Omega^q} \sum_{c=1}^{n} \hat{\theta}^c \mathbf{P}^{cT}(\mathbf{x}) \left(\mathbf{S} \sum_{a=1}^{n} \mathbf{P}^a(\mathbf{x}) \hat{\phi}^a + \mathbf{Z} \sum_{a=1}^{n} \mathbf{P}^a(\mathbf{x}) \hat{\theta}^a \right) d\Omega = - \int_{\Gamma^q_\Lambda} \bar{\Lambda} d\Gamma \end{aligned} \tag{69}$$

$$\int_{L^q + \Gamma^q_\phi} \mathbf{N}(\mathbf{x}) \left(\mathbf{S} \sum_{a=1}^{n} \mathbf{P}^a(\mathbf{x}) \hat{\phi}^a + \mathbf{Z} \sum_{a=1}^{n} \mathbf{P}^a(\mathbf{x}) \hat{\theta}^a \right) d\Gamma = \int_{\Gamma^q_Q} \bar{Q} d\Gamma . \tag{70}$$

This system can be solved iteratively as

Preprints (www.preprints.org) | NOT PEER-REVIEWED | Posted: 6 May 2020 doi:10.20944/preprints202005.0095.v1

Peer-reviewed version available at Materials 2020, 13, 2527; doi:10.3390/ma13112527

$$\int_{L^q+\Gamma_\theta^q}\left[\left(l^2\mathbf{F}_\theta(\mathbf{x})\sum_{a=1}^{n}\mathbf{P}^a_{,kk}(\mathbf{x})-\bar{\mathbf{F}}_\theta^{(k-1)}(\mathbf{x})\sum_{a=1}^{n}\mathbf{P}^a(\mathbf{x})\right)\hat{\theta}^{a(k)}-\bar{\mathbf{F}}_\phi^{(k-1)}(\mathbf{x})\sum_{a=1}^{n}\mathbf{P}^a(\mathbf{x})\hat{\phi}^{a(k)}\right]d\Gamma+$$

$$+l^2\left(n_k(\mathbf{x}^s_\Lambda)\mathbf{F}_\mu(\mathbf{x}^s_\Lambda)\sum_{a=1}^{n}\mathbf{P}^a_{,k}(\mathbf{x}^s_\Lambda)-n_k(\mathbf{x}^f_\Lambda)\mathbf{F}_\mu(\mathbf{x}^f_\Lambda)\sum_{a=1}^{n}\mathbf{P}^a_{,k}(\mathbf{x}^f_\Lambda)\right)\hat{\theta}^{a(k)}- \tag{71}$$

$$-\int_{\Omega^q}\sum_{c=1}^{n}\hat{\theta}^{c(k-1)}\mathbf{P}^{cT}(\mathbf{x})\left(\mathbf{S}\sum_{a=1}^{n}\mathbf{P}^a(\mathbf{x})\hat{\phi}^{a(k)}+\mathbf{Z}\sum_{a=1}^{n}\mathbf{P}^a(\mathbf{x})\hat{\theta}^{a(k)}\right)d\Omega=-\int_{\Gamma_\Lambda^q}\bar{\Lambda}d\Gamma$$

$$\int_{L^q+\Gamma_\phi^q}\mathbf{N}(\mathbf{x})\left(\mathbf{S}\sum_{a=1}^{n}\mathbf{P}^a(\mathbf{x})\hat{\phi}^{a(k)}+\mathbf{Z}\sum_{a=1}^{n}\mathbf{P}^a(\mathbf{x})\hat{\theta}^{a(k)}\right)d\Gamma=\int_{\Gamma_Q^q}\bar{Q}d\Gamma\ , \tag{72}$$

with ($k=1,2,\ldots$), $\hat{\theta}^{a(0)}=0$, $\hat{\phi}^{a(0)}=0$ and

$$\bar{\mathbf{F}}_\theta^{(k-1)}(\mathbf{x})=\left[n_1(\mathbf{x})\bar{\kappa}_{11}^{(k-1)}(\mathbf{x})\quad n_2(\mathbf{x})\bar{\kappa}_{22}^{(k-1)}(\mathbf{x})\right],$$

$$\bar{\mathbf{F}}_\phi^{(k-1)}(\mathbf{x})=\left[n_1(\mathbf{x})\bar{\zeta}_{11}^{(k-1)}(\mathbf{x})\quad n_2(\mathbf{x})\bar{\zeta}_{22}^{(k-1)}(\mathbf{x})\right],$$

where $\bar{\kappa}_{ij}^{(k-1)}(\mathbf{x})=\left(\kappa_{ij}+\alpha^2 s_{ij}(T_0+\theta^{(k-1)}(\mathbf{x}))\right)$, $\bar{\zeta}_{ij}^{(k-1)}(\mathbf{x})=\zeta_{ij}\left(T_0+\theta^{(k-1)}(\mathbf{x})\right)$.

3.2 Numerical examples

An axially symmetric thermoelectric problems, as shown in Fig. 6, is analysed in the example. The thermoelectric material Bi_2Te_3, is considered. It has the following material constants (Yang et al. 2014) with isotropic properties:

$$s=1.1\times10^5 Am/V\,,\qquad \alpha=\zeta/s=2\times10^{-4}\mathrm{V}^2/KAm\,,\qquad \kappa=1.6W/Km\ . \tag{73}$$

Characteristic length for the selected material structure is $l=5\times10^{-9}m$.

Following geometry of the hollow cylinder is considered: internal radius r_1=1e-7 m and external radius r_2=2.5e-7 m. Vanishing values of electric potentials are prescribed on inner and external surfaces. Also vanishing values of the temperature gradients on both surfaces are considered.

Preprints (www.preprints.org) | NOT PEER-REVIEWED | Posted: 6 May 2020 doi:10.20944/preprints202005.0095.v1

Peer-reviewed version available at Materials 2020, 13, 2527; doi:10.3390/ma13112527

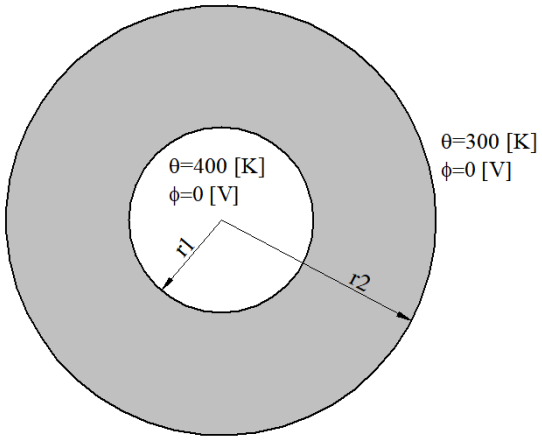

Fig. 6: Geometry and boundary conditions

The coupled thermo-electric problem is analyzed numerically. The influence of the tube thickness $L = r_2 - r_1$ on temperature and induced electric potential is investigated. Numerical results are presented in Figures 7 and 8. The induced electric potential grows with increasing the value *l/L*. In classical thermoelectricity, it is possible to find the analytical solution.

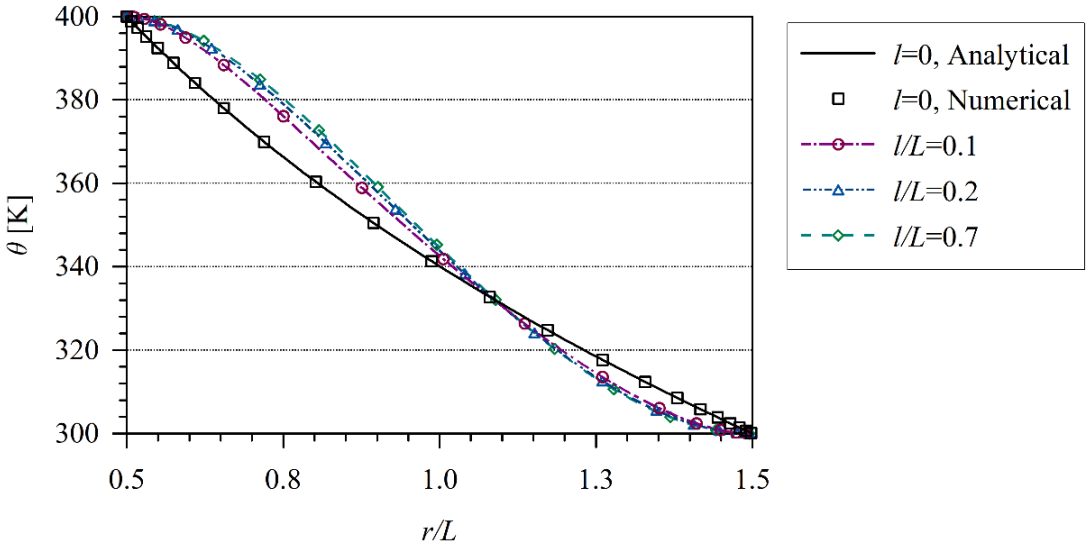

Fig. 7: Temperature variation along non dimensional *x/L* coordinate in hollow cylinder

Preprints (www.preprints.org) | NOT PEER-REVIEWED | Posted: 6 May 2020 doi:10.20944/preprints202005.0095.v1

Peer-reviewed version available at Materials 2020, 13, 2527; doi:10.3390/ma13112527

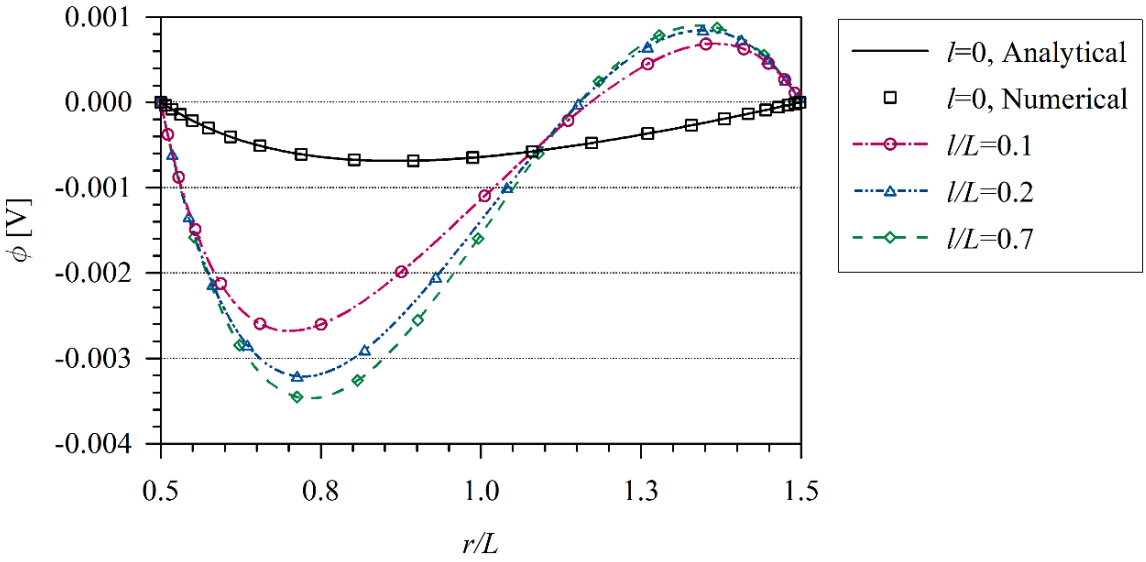

Fig. 8: The electric potential variation along non dimensional *x/L* coordinate in hollow cylinder

4 Conclusions

The meshless Petrov-Galerkin (MLPG) method has been successfully applied to multiphysical problems described by advanced continuum models with microstructural effects. Strain- and electric intensity vector – gradients are considered in constitutive equations for electric displacement and stresses in flexoelectricity, respectively. Similarly, the constitutive equations for thermoelectric materials contain higher order derivatives of temperature in the higher-grade heat conduction theory. It allows to describe the heat transfer more realistic in nanostructures. The governing equations are derived for both multiphysical problems, where size effects are considered. These equations contain higher order derivatives of physical fields than in the classical continuum models. Application of classical domain discretization methods to corresponding boundary value problems brings some difficulties with continuity of approximated fields.

The proposed MLPG computational method with the MLS approximation of fields is very convenient to solve governing equations of gradient theory with high-order derivatives. The order of continuity of the MLS approximation can be tuned to a desired value very easily. Therefore, the present computational method is promising to be applied to multiphysical problems described by gradient theories.

Acknowledgement

The authors acknowledge the support by the Slovak Science and Technology Assistance Agency registered under number APVV-18-0004 and VEGA-2/0061/20.

References

1. Buhlmann, S.; Dwir, B.; Baborowski, J.; Muralt, P. Size effects in mesoscopic epitaxial ferroelectric structures: increase of piezoelectric response with decreasing feature-size. *Appl. Phys. Lett.* **2002**, 80, 3195-3197.
2. Cross, LE. Flexoelectric effects: charge separation in insulating solids subjected to elastic strain gradients. *J. Mater. Sci.* **2006**, 41, 53-63.
3. Harden, J.; Mbanga, B.; Eber, N.; Fodor-Csorba, K.; Sprunt, S.; Gleeson, JT.; Jakli, A. Giant flexoelectricity of bent-core nematic liquid crystals. *Phys. Rev. Lett.* **2006**, 97, 157802.
4. Zhu, W.; Fu, JY.; Li, N.; Cross, LE. Piezoelectric composite based on the enhanced flexoelectric effects. *Appl. Phys. Lett.* **2006**, 89: 192904.
5. Catalan, G.; Lubk, A.; Vlooswijk, AHG.; Snoeck, E.; Magen, C.; Janssens, A.; Rispens, G.; Rijnders, G.; Blank, DHA.; Noheda, B. Flexoelectric rotation of polarization in ferroelectric thin films. *Nat. Mater.* **2011**, 10, 963-967.
6. Kogan, SM. Piezoelectric effect during inhomogeneous deformation and acoustic scattering of carriers in crystals. *Sov. Phys. Solid State* **1964**, 5, 2069-2070.
7. Meyer, RB. Piezoelectric effects in liquid crystals. *Phys. Rev. Lett.* **1969** 22, 918-921.
8. Sharma, P.; Maranganti, R.; Sharma, ND. On the possibility of piezoelectric nanocomposites without using piezoelectric materials. *J. Mech. Phys. Solids* **2007**, 55, 2328-2350.
9. Deng, Q.; Liu, L.; Sharma, P. Flexoelectricity in soft materials and biological membranes. *J. Mech. Phys. Solids* **2014**, 62, 209–227.
10. Landau, LD.; Lifshitz, EM. *Electrodynamics of Continuous Media*, 2nd Ed. Butterworth-Heinemann, 358-371,**1984**.
11. Yang, JS. Effects of electric field gradient on an antiplane crack in piezoelectric ceramics. *Int. J. Fracture* **2004**, 127: L111-L116.
12. Yang, XM.; Hu, YT.; Yang, JS. Electric field gradient effects in anti-plane problems of polarized ceramics. *Int. J. Solids Struct.* **2004**, 41: 6801-6811.
13. Hicks, L.; Dresselhaus, MS. Thermoelectric figure of merit of a one-dimensional conductor. *Phys. Rev. B* **1993**, 47, 16631.
14. Minnich, AJ.; Dresselhaus, MS.; Ren, ZF.; Chen, G. Bulk nanostructured thermoelectric materials: current research and future prospects. *Energy Envir. Sci.* **2009**, 2, 466-479.
15. Eringen, AC. Non-local polar field theory. In: Eringen A.C., editor. *Continuum Physics*, vol. 4., Academic Press, New York , 1976.
16. Mindlin, RD. Micro-structure in linear elasticity. *Arch. Ration. Mech. Anal.* **1964**, 16: 51–78.

17. Mindlin, RD. Second gradient of strain and surface-tension in linear elasticity. *Int. J. Solids Struct.* **1965**, 1, 417–438.
18. Aifantis, E. On the microstructural origin of certain inelastic models. *ASME J. Eng. Mater. Technol.* **1984**, 106, 326–330.
19. Allen, PB. Size effects in thermal conduction by phonons. *Phys. Rev. B* **2014**, 90, 054301.
20. Deng, F.; Deng, Q.; Yu, W.; Shen, S. Mixed finite elements for flexoelectric solids. *J. Appl. Mech.* **2017**, 84, 081004.
21. Dong, L.; Atluri, S.N. A simple procedure to develop efficient & stable hybrid/mixed elements, and Voronoi cell finite elements for macro- & micromechanics. *CMC: Computers, Materials & Continua* **2011**, 24, 61–104.
22. Atluri, SN. *The Meshless Method (MLPG) for Domain and BIE Discretizations.* Tech Science Press, Forsyth, 2004.
23. Sladek, J.; Stanak, P.; Han, ZD.; Sladek, V.; Atluri, SN. Applications of the MLPG method in engineering & Sciences: A review. *CMES: Computer Modeling Engn. & Sci.* **2013**, 92, 423-475.
24. Sladek, J.; Sladek, V.; Repka, M.; Kasala, J.; Bishay, P. Evaluation of effective material properties in magneto-electro-elastic composite materials. *Composite Struct*. **2017**, 109, 176-186.
25. Maranganti, R.; Sharma, ND.; Sharma, P. Electromechanical coupling in nonpiezoelectric materials due to nanoscale nonlocal size effects: Green's function solutions and embedded inclusions. *Phys. Rev. B* **2006**, 74, 014110.
26. Hu, SL.; Shen, SP. Electric field gradient theory with surface effect for nano-dielectrics. *CMC: Computers, Materials & Continua* **2009**, 13, 63-87.
27. Altan, S.; Aifantis, E. On the structure of the mode III crack-tip in gradient elasticity. *Scripta Metall. Mater.* **1992**, 26, 319–324.
28. Askes, H.; Aifantis, E. Gradient elasticity in statics and dynamics: An overview of formulations, length scale identification procedures, finite element implementations and new results. *Int. J. Solids Struct.* **2011**, 48, 1962-1990.
29. Gitman, I.; Askes, H.; Kuhl, E.; Aifantis, E. Stress concentrations in fractured compact bone simulated with a special class of anisotropic gradient elasticity. *Int. J. Solids Struct.* **2010** 47, 1099-1107.
30. Yaghoubi, ST.; Mousavi, SM.; Paavola, J. Buckling of centrosymmetric anisotropic beam structures within strain gradient elasticity. *Int. J. Solids Struct.* **2017,** 109, 84-92.
31. Sladek, J.; Sladek, V.; Wunsche, M.; Zhang, Ch. Effects of electric field and strain gradients on cracks in piezoelectric solids. *Eur. J. Mechanics/A Solids* **2018**, 71, 187–198.

32. Sladek, J.; Sladek, V.; Repka, M.; Schmauder S. Mixed FEM for quantum nanostructured solar cells. *Composite Struct.* **2019**, 229, 111460.
33. Yang, Y.; Gao, C.; Li, J. The effective thermoelectric properties of core-shell composites. *Acta Mechanica* **2014**, 225, 1211-1222.